

## Corresponding Author:

Urszula Szczepaniak, IRsweep AG, Laubisruetistrasse 44, 8712 Staefa, Switzerland

Email: urszula.szczepaniak@irsweep.com

# Vibrational Stark Spectroscopy on Fluorobenzene with Quantum Cascade Laser Dual Frequency Combs

Urszula Szczepaniak<sup>1</sup>, Samuel H. Schneider<sup>2</sup>, Raphael Horvath<sup>1</sup>, Jacek Kozuch<sup>2</sup>, Markus Geiser<sup>1</sup>

<sup>1</sup> IRsweep AG, Laubisruetistrasse 44, 8712 Staefa, Switzerland

<sup>2</sup> Department of Chemistry, Stanford University, Stanford, California 94305-5012

## Abstract

We demonstrate the performance of a dual frequency comb QCL spectrometer for the application of vibrational Stark spectroscopy. Measurements performed on fluorobenzene with the dual-comb spectrometer were compared to results obtained using a conventional Fourier transform infrared (FTIR) instrument in terms of spectral response, parameter estimation, and signal-to-noise ratio. The dual-comb spectrometer provided the same qualitative and quantitative data as the FTIR setup with an up to 9 or 52 times improved signal to noise ratio (SNR) in the current configuration when comparing against experimental or acquisition times, respectively. This improvement was made possible by the shorter experimental and acquisition times, and the brighter light-source. Additional characteristics of the dual-comb spectrometer applicable to vibrational Stark spectroscopy and their scaling properties for future applications are discussed.

## Keywords

Vibrational Stark Spectroscopy, VSS, Frequency Combs, Quantum Cascade Lasers, IRsweep

## Introduction

The influence of electric fields on optical spectra is known as the Stark effect or electrochromism.<sup>1</sup> While it has been extensively exploited in electronic spectroscopy<sup>2–6</sup>, similar effects can also be observed in vibrational spectra<sup>7,8</sup>, i.e. the vibrational Stark effect (VSE), where an electric field perturbs a vibrational mode's ground and excited states, resulting in a shift of its absorption energy. This effect has been used in the study of proteins<sup>9–11</sup> and other biological systems<sup>12–14</sup>, electrode interfaces<sup>15–17</sup>, solute-solvent interactions<sup>18</sup> etc., providing insight into the nature of electrostatics on the molecular level, a topic of general importance in biology, chemistry, and materials science<sup>19</sup>. In this way, it has contributed towards understanding the effect of electric fields on the anharmonicity of

chemical bonds, the band structure in materials, binding and catalytic processes, as well as on the transition state stabilization in enzymes; the latter is particularly relevant in the field of protein design and engineering, and its applications in biocatalysis.<sup>19</sup>

The framework of the VSE enables quantification of the magnitude of electric fields or their changes using suitably calibrated vibrational probes, e.g. local high frequency modes such as carbonyls and nitriles. Vibrational Stark spectroscopy (VSS) is an experimental approach to directly measure the sensitivity of a vibrational mode to an external electric field, providing such a quantitative calibration for inferring electric fields in condensed phase systems using vibrational spectroscopy (e.g. Fourier-Transform Infrared (FTIR), Raman, 2D-IR, etc.).<sup>7,20–24</sup> It is generally performed in an isotropic frozen glass, where the change in absorbance in the presence and absence of an electric field can be related to the derivatives of the absorbance spectrum in the absence of an external field. High frequency local modes are generally observed to follow the linear Stark effect<sup>8</sup>. That is, their response to an electric field arises predominantly from the difference dipole, referred to as the Stark tuning rate ( $\Delta\mu = \mu_1 - \mu_0$ ; units of  $\text{cm}^{-1}/(\text{MV}/\text{cm})$ ), between the ground and first-excited states of the vibrational mode. In VSS, analysis of the 2nd-derivative contribution to the observed field-on minus field-off spectrum can be directly used to quantify the Stark tuning rate. Usually, the VSS spectra in the mid-IR region are probed with the use of Fourier transform infrared (FTIR) instruments.<sup>19</sup> While suitable for a variety of possible applications, the approach is currently limited to the analysis of small molecules with high solubility (ca.  $\geq 100$  mM) in an appropriate frozen polymer or glassy matrix where high signal-to-noise ratios (SNR) can be achieved. This limitation is brought about mainly by the low brightness of commonly used IR light sources in FTIR spectrometers in combination with the low sensitivity of the VSS signal, the low oscillator strength (in comparison to many electronic transitions) and the isotropy of the frozen sample. Consequently, the low brightness of FTIR globars naturally results in long experimental durations, which can potentially increase the likelihood of dielectric breakdown from the externally applied electric field. Therefore, a rapid technique with a high-power polychromatic source in the mid-IR is sought.

We present VSS measurements on a fluorobenzene sample using a new high-brightness, high-speed, and multi-wavelength dual-comb spectrometer (DCS) based on quantum cascade laser (QCL) dual frequency combs in the  $1180 - 1230 \text{ cm}^{-1}$  range. Generating frequency combs in mid-infrared region is a challenging task.<sup>25</sup> Thanks to the discovery of a semiconductor QCL-based electrically pumped frequency-comb source<sup>26</sup>, dual-comb mid-IR spectroscopy systems were substantially simplified.<sup>27,28</sup> The spectral spacing of comb modes of  $0.3 \text{ cm}^{-1}$  exceeds the requirements for studies of solids or fluids. The results are compared to those obtained with a conventional FTIR spectrometer and we speculate on future considerations and outlook regarding the expanded experimental scope accessible via DCS-based spectrometers for VSS.

## Experimental

### Sample preparation

Solutions of 100 mM fluorobenzene (Sigma Aldrich, Inc.; see Figure 1) in 2-methyltetrahydrofuran (ACROS Organics) were prepared for both FTIR and dual comb spectroscopy measurements. The inner surfaces of  $\text{CaF}_2$  (1 mm thickness, 12.7 mm

diameter, FOCtek Photonics) windows were coated with 4.5 nm of Ni, which acts as an electrode in the experiments. The sample was placed between two electrode-coated windows offset with ca. 25  $\mu\text{m}$  Teflon spacers and immersed in home-built liquid nitrogen cryostat<sup>29</sup> equipped with IR-transparent windows to form an isotropic frozen glass. The capacitor thickness was determined using interferometry. The voltage was applied with a Trek 10/10 high-voltage power amplifier. Further spectrometer-specific experimental details are outlined below.

## Dual Frequency-Comb Spectroscopy

Experiments were performed with a table-top dual frequency comb spectrometer (IRsweep IRis-F1).<sup>30,31</sup> The dual-comb system (Figure 1 – left) is based on two free-running quantum cascade laser (QCL) frequency combs that individually span over 70  $\text{cm}^{-1}$  and are centered at  $\sim 1220 \text{ cm}^{-1}$ .<sup>32</sup> The combs overlap in the 1180 to 1230  $\text{cm}^{-1}$  region which results in dual-comb absorption spectra covering 55  $\text{cm}^{-1}$  with 0.3  $\text{cm}^{-1}$  sampling. The average power per comb tooth is  $>2 \text{ mW}$  with a total continuous wave output power of about 700 mW. The laser beams are combined, split into two beams on a 50:50  $\text{CaF}_2$  beam splitter and attenuated with neutral density filters. One of the combined beams is focused on a high-bandwidth HgCdTe reference detector, while the other passes through the sample (beam size of ca. 4 mm) and is then detected by a second identical HgCdTe detector.

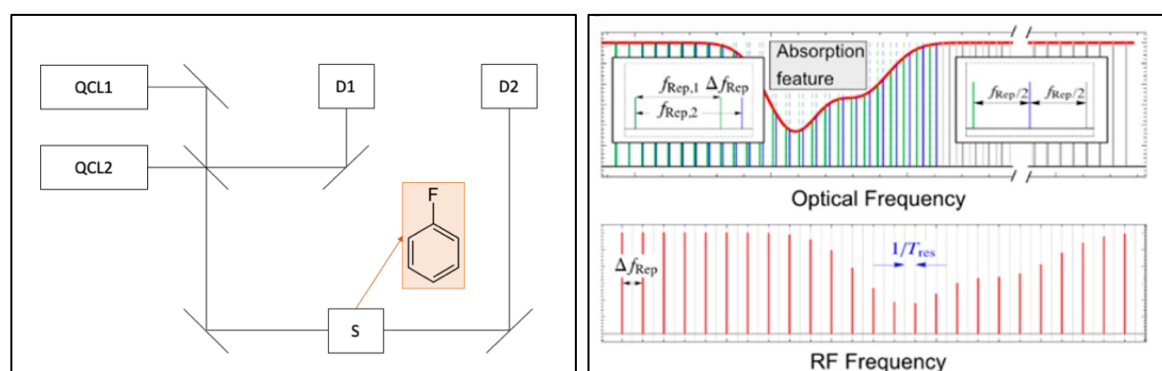


Figure 1. Left: Setup for dual-comb spectroscopy. Two quantum cascade lasers (QCL1, QCL2) generate frequency combs that travel (i) to a fast AC-coupled HgCdTe detector (D1) (ii) through sample compartment (S) with an optically active sample (fluorobenzene) to an identical HgCdTe detector (D2). Right: Top panel: Representation of two frequency combs with slightly differing repetition frequencies ( $f_{\text{Rep},1}$ ,  $f_{\text{Rep},2}$ ). Bottom: Beating signal of the interleaving combs shown in the top panel. Information from optical range is mapped onto the radio frequency range. Adapted from Ref. 30.

Overlapping two frequency combs allows simultaneous detection of the optical modes of the lasers due to a multi-heterodyne detection scheme. The mixing of two frequency-combs (Figure 1 – right top) results in a heterodyne beat spectrum with the frequency spacing between beatings of neighboring comb teeth in the radio frequency range (Figure 1 – right bottom):  $\Delta f_{\text{Rep}} = f_{\text{Rep},1} - f_{\text{Rep},2}$ , where  $f_{\text{Rep},1}$  and  $f_{\text{Rep},2}$  are repetition frequencies of the lasers 1 and 2, respectively. The achievable time resolution, connected with resolving neighboring comb teeth, is limited by  $\Delta f_{\text{Rep}}$ , according to the relation:  $T_{\text{res}} = 2/\Delta f_{\text{Rep}}$ . Due to high repetition rate of the used QCLs, enabled by a low cavity length, short acquisition time and high time resolution ( $<1 \mu\text{s}$ ) can be achieved.<sup>30</sup>

Figure 2A shows the triggering schematic of the experiment. In the dual-comb experiment, the voltage was controlled with a trigger; data were acquired for 16 ms, consisting of 8 ms with voltage on and 8 ms with voltage off. This *acquisition time per cycle*, where one cycle refers to one acquired difference spectrum, multiplied by the number of acquisitions, is later referred to as *the acquisition time*. The trigger signals were separated in time by 1 s, yielding 1 s cycles (i.e. *experimental time per cycle*) and defining *the experiment time* as multiplication of number of acquisitions by 1 s. The Stark spectra are obtained by calculating the difference in sample absorption in the presence and absence of an externally applied electric field with upwards of 96 spectra being averaged. The low-temperature absorbance spectrum required for Stark analysis and wavenumber calibration were performed with an FTIR. Two sets of voltages were applied: 2.0 kV, and 3.0 kV, to a  $28.0 \pm 0.1 \mu\text{m}$  thick sample, corresponding to fields of 0.715 MV/cm, and 1.073 MV/cm, respectively. It was verified that the Stark signal scales with a square of the electric field intensity.<sup>19</sup>

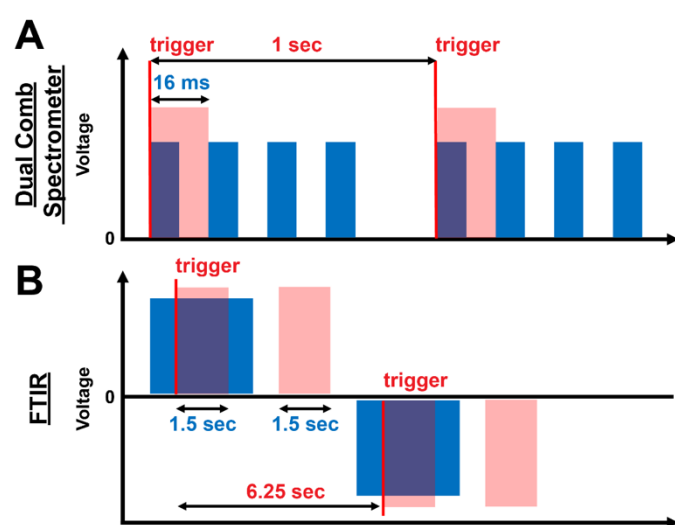


Figure 2. Schematic of a triggered experiment. (A) Dual-comb spectrometer. (B) FTIR. Blue areas indicate time when the voltage was applied, red areas indicate acquisition time. Time between the two vertical red lines, denoted by “trigger”, indicates experimental time per cycle (red number). Acquisition time is indicated by the time (blue numbers) shown between each “trigger”. Not drawn to scale, see text for further details.

## Fourier Transform Infrared Spectroscopy

The FTIR measurements were performed with a Bruker Vertex 70 FTIR spectrometer equipped with a global source and a liquid nitrogen-cooled HgCdTe detector. Spectra were measured with  $1.0 \text{ cm}^{-1}$  resolution and 128 scans (field on - field off) were averaged. A similar principle of taking difference spectra as for dual-comb spectrometer measurements was used here. The cycles were realized as presented in Figure 2B. The *experimental time per cycle* was 6.25 s and yielded a total *experiment time* of 800 s. Each cycle constituted an acquisition time of 3 s resulting from 1.5 s of data acquisition per field-on or field-off scan. The applied voltage was 2.07 kV, and the sample thickness  $27.78 \pm 0.03 \mu\text{m}$ , yielding a field of 0.745 MV/cm. The resulting interferograms were transformed into absorbance spectra using a Blackman-Harris 3-Term apodization function in the range of  $4000\text{-}1000 \text{ cm}^{-1}$  with a phase resolution of 32 and a zero-filling factor of 2. Note that these measurements are

operating at ca. 8000 ADC counts at a maximum aperture of 6 mm accessible via FTIR, which equates to ca. 1/3 of the maximum peak light intensity that can be detected by the HgCdTe detector for optimal SNR.

To assure a well-defined absorption lineshape (both good SNR and accuracy in the wings required for further use of the derivatives; see later in text), the sample absorption for both spectrometer analyses was measured in the same FTIR configuration after successful Stark spectra were recorded and is a potential source of deviation in the Stark tuning rate determination presented below. Immersing the sample in liquid N<sub>2</sub> results in an error in absorbance readout of about  $\pm 0.01$  absorbance units.<sup>19</sup> The FTIR spectra were recorded and extracted with the use of commercially available software (Bruker OPUS 5.5).

## Data Analysis

In conducting the data analysis, we compare two parameters between DCS and FTIR: the raw spectral SNR and the Stark tuning rate from analytical fitting. For the comparison we used the Stark spectra measured at comparable electric fields, i.e. 0.715 and 0.745 MV/cm<sup>-1</sup> in the case of the DCS and FTIR spectra, respectively.

The SNR was determined as  $SNR = \frac{Fitted\ Signal_{max} - Fitted\ Signal_{min}}{weighted\ error}$ , where the numerator corresponds to the signal intensity (i.e. the maximum difference signal) in the measurement and  $weighted\ error = \frac{\sum_i(w_i \cdot error_i)}{\sum_i(w_i)}$ . In the latter expression,  $w_i$  is the weighting factor at a given spectral point. The quantity  $error_i$  is the error inherent in a spectral point and due to the different spectral characteristics of the two spectrometers it is calculated differently for DCS and FTIR. Both  $error_i$  and  $w_i$  were calculated as outlined below.

For FTIR,  $error_i$  is equal to the RMSE (root mean squared error), calculated for a linear fit of the spectral region without spectral features, and the weights,  $w_i$ , were set to unity, owing to the relatively flat power distribution of the thermal source used for FTIR in this region of the spectrum. However, this approach is unsuitable for DCS, since the laser intensity, and by extension the SNR, varies strongly across the spectrum and therefore using an arbitrary (i.e. spectrally flat) region to perform the noise analysis would lead to a skewed result.

A property of the data treatment in DCS is that a standard deviation for each spectral line is derived from the time-dependent signal on the reference detector. This value is used for  $error_i$  for the DCS analysis. The weights,  $w_i$ , are then the inverse variance of the signal for DCS. Weighting is made possible by this time-dependent error analysis and is commonly used in spectral averaging of DCS data.<sup>30</sup> In DCS, each spectral data point should be weighted according to its noise properties, since only then the physical properties and the stability of DCS system are reflected.

The Stark tuning rate was independently determined for the FTIR and DCS data through a non-linear curve fitting procedure summarized below. The details of the fitting procedure and the corresponding parts of Python scripts used for the evaluation are shown in the SI. At first, the absorbance peak of fluorobenzene (A; recorded by FTIR and expressed in units of extinction coefficient, i.e. M<sup>-1</sup> cm<sup>-1</sup>) was fit with a pseudo-Voigt profile yielding a function of wavenumber ( $\tilde{\nu}$ ), i.e.  $A(\tilde{\nu})$ . The first and second derivatives of the quotient absorbance and the wavenumber  $A(\tilde{\nu})/\tilde{\nu}$  were calculated. The Stark data (both FTIR and DCS also in units of extinction coefficient) were normalized by the applied field and then independently fit with a weighted global fit to the curve:  $\Delta A = aA(\tilde{\nu}) + b \frac{d}{d\tilde{\nu}} \frac{A(\tilde{\nu})}{\tilde{\nu}} + c \frac{d^2}{d^2\tilde{\nu}} \frac{A(\tilde{\nu})}{\tilde{\nu}}$ . Coefficients  $a$ ,  $b$ , and  $c$  were found through a weighted non-linear least squares minimization (*curve\_fit* function

of Python library *scipy*). Again, the inverse variance was used as weights for fitting the DCS data (see details in the function description, available also in the SI). The fitting procedure yielded the value of  $c$ , as well as the covariance matrix from which the standard deviation of  $c$  ( $\sigma_c$ ) could be determined. The Stark tuning rate was obtained as,  $\Delta\mu = \sqrt{10}c^{33}$  and its uncertainty (see Figure 3) was taken as  $\sqrt{10}\sigma_c$ .

This approach ensures that the SNR is independent of the spectral region in which the signal is recorded. Using another sample of similar signal strength but absorbing in a noisier part of the DCS spectrum would still lead to the same SNR, but a greater uncertainty in the fitting coefficients due to weighting of the spectral signal.

## Results and Discussion

### Determination of the Stark tuning rate of fluorobenzene

Data from the DCS and FTIR produce the same pronounced second-derivative-like Stark lineshape, as shown in Figure 3, and are in accordance with previously reported spectra centered at  $1214.2\text{ cm}^{-1}$ .<sup>34</sup> The determined Stark tuning rate values ( $|\Delta\mu|f$ ) are  $(0.75 \pm 0.09)$  and  $(0.89 \pm 0.18)\text{ cm}^{-1}/(\text{MV}/\text{cm})$  from the DCS and FTIR, respectively. These values are in agreement with each other when considering the determined error margins, which are smaller for the DCS-derived value with an uncertainty of 12 %, as compared to 20 % for the FTIR. The observed difference of both absolute magnitudes (i.e. 0.75 and  $0.89\text{ cm}^{-1}/(\text{MV}/\text{cm})$ ) can be rationalized either based on manual inconsistencies in the baselining of the FTIR-obtained Stark spectra or deviations in the sample thickness between room temperature and 77 K, at which the thickness was determined and the VSS experiment was performed, respectively. According to Bublitx and Boxer<sup>19</sup> the latter can result in errors of  $\pm 1\text{-}2\text{ }\mu\text{m}$ . Nevertheless, both values are in accordance within the determined error margins of that previously measured<sup>34</sup> for the C-F stretch of fluorobenzene in 2-methyltetrahydrofuran, i.e.  $|\Delta\mu|f = 0.84\text{ cm}^{-1}/(\text{MV}/\text{cm})$ .

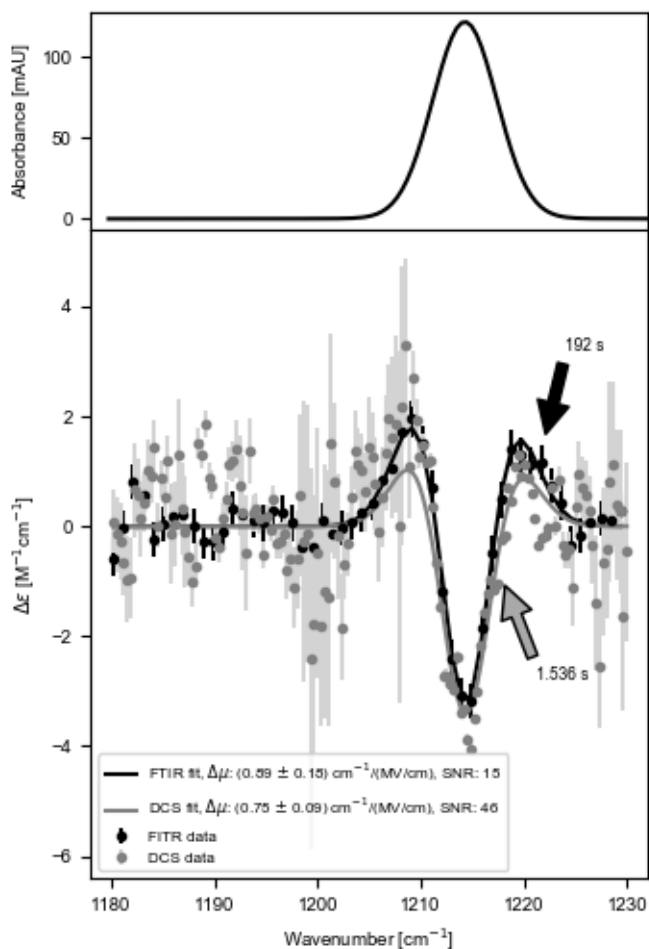


Figure 3. Top: IR absorption spectrum of 100 mM fluorobenzene in glassy 2-MeTHF at 77K. Bottom: Stark spectra scaled to an electric field strength of 1 MV/cm as registered with dual-comb spectrometer (grey, after total acquisition time of 1.536 s, equivalent to 96 cycles with a spectral sampling of  $0.3 \text{ cm}^{-1}$ ) and FTIR (black, after total acquisition time of 384 s, equivalent to 128 cycles at a spectral resolution of  $1 \text{ cm}^{-1}$ ). Error bars correspond to standard deviation of the laser line intensity (DCS) and RMSE of the linear fit determined for the part of the spectrum below  $1200 \text{ cm}^{-1}$  (FTIR). Data fitted with linear combination of absorbance derivatives (see text). For details on  $\Delta\mu$  and SNR determination see text.

The DCS spectra presented in Figure 3 were recorded with an experiment time of 96 s, of which 1.536 s was the acquisition time. Even shorter times can be sufficient to obtain the information of interest. In order to test the sensitivity of the set-up we compared the spectra for various acquisition times. Figure 4 presents Stark spectra as registered for 8 to 96 averages, corresponding to 128 ms to 1.536 s acquisition time, and to 8 s to 96 s experiment time, respectively. The Stark response can be observed with acquisition times as short as 128 ms.



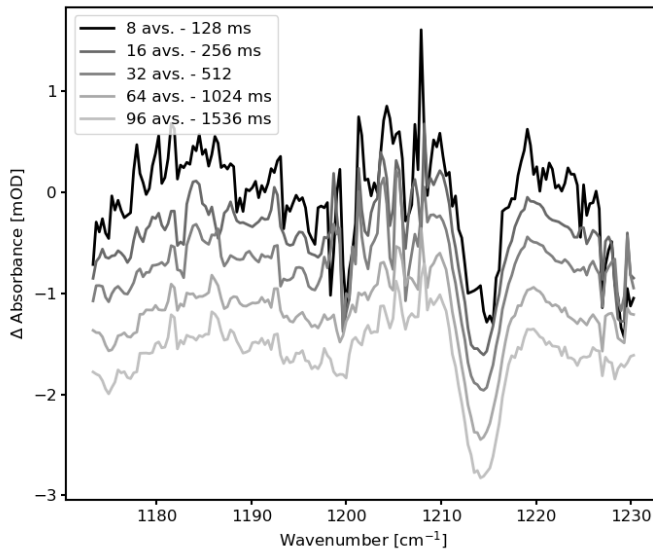


Figure 4. Stark spectra obtained with DCS with increasing averaging and corresponding acquisition times, measured at an external electric field of 1.07 MV/cm and with a spectral sampling of 0.3 cm<sup>-1</sup>. No smoothing applied. Offset of 0.4 mOD used for better visualization of the curves.

## Signal-to-Noise Ratio (SNR) analysis I – Normalization to experiment time

Accounting for the wavelength-dependent noise characteristics of the DCS spectrum we obtain SNR values of 46 and 15 for the DCS and FTIR spectra, respectively, as shown in Figure 3. After normalization of these values for the experiment time (i.e. 96 s or 800 s, respectively) and the applied fields (of 0.715 and 0.745 MV/cm; note that the signal scales with field squared) a final ratio of SNR values of

$$\frac{SNR_{DCS}}{SNR_{FTIR}} = \frac{SNR_{DCS,raw}}{SNR_{FTIR,raw}} \cdot \frac{\sqrt{\text{time}_{FTIR}}}{\sqrt{\text{time}_{DCS}}} \cdot \left(\frac{F_{FTIR}}{F_{DCS}}\right)^2 = \frac{46}{15} \cdot \frac{\sqrt{800 \text{ s}}}{\sqrt{96 \text{ s}}} \cdot \left(\frac{0.745 \frac{MV}{cm}}{0.715 \frac{MV}{cm}}\right)^2 = 9.6 \quad (1)$$

is achieved. From Figure 3 it can be seen that the C-F stretching band is located in the low-noise region of the DCS spectrum. However, it should be noted that this is not the origin of the observed improvement of SNR, since the noise was calculated for the whole spectral window covered by DCS. The location of the low noise region only affects the estimated value (the Stark tuning rate) and its uncertainty. Lasers in other spectral regions (e.g. amide I band) can have a more homogeneous power distribution leading to a less wavelength-dependent noise level throughout the covered spectral range.

## Signal-to-Noise Ratio (SNR) analysis II – Normalization to acquisition time

As shown in Figure 2, different experiment and acquisition times are resulting in one cycle of accumulation with both instruments. In the case of the FTIR, one cycle has a duration of 6.25 s, of which 3 s are used to detect the signal (acquisition time) and 3.25 s to process the



data. In contrast, using the DCS, one 1 s cycle consisted of 16 ms acquisition time and 984 ms being in part waiting time due to the trigger settings and in part time for reading and saving the data, split approximately half-half. The latter acquisition scheme was chosen at the time the experiments were performed since the DCS was optimized for single shot experiments reported previously.<sup>30,31</sup> However, it is the most obvious aspect for future improvement and current attempts are focused on improving the balance between acquisition and “dead time”. It is therefore interesting to compare the SNR values of both instruments in terms of *acquisition time*. Such a comparison is not only relevant as a future outlook to compare optimal acquisition schemes, but is also for cases where single shot experiments can or have to be performed due to high signal-to-noise levels or experimental constraints of the sample of interest. In VSS, this latter concern is exemplified by the constant risk of dielectric breakdown which can occur at any point when high voltages are applied. We discuss further implications in the following sections. In these cases the observed ratio of SNR values of 46/15 for DCS/FTIR, extracted from the spectra in Figure 3,

needs to be normalized using a factor of  $\frac{\sqrt{\text{time}_{FTIR}}}{\sqrt{\text{time}_{DCS}}} \cdot \left(\frac{F_{FTIR}}{F_{DCS}}\right)^2 = \frac{\sqrt{384 \text{ s}}}{\sqrt{1.536 \text{ s}}} \cdot \left(\frac{0.745 \frac{\text{MV}}{\text{cm}}}{0.715 \frac{\text{MV}}{\text{cm}}}\right)^2 = 17.1$

resulting in an improved SNR by a factor of 52.6 using the DCS. The results of both normalizations are presented in Table 1.

Table 1. The results of SNR analysis and auxiliary data for spectra obtained with FTIR and dual-comb spectrometer instruments. The plotted spectra are presented in Figure 3. One cycle is defined as 1 scan field-on followed by 1 scan field-off together with connected processing time before the next measurement with field on begins.

	FTIR	Dual-comb spectrometer
SNR, raw	15	46
Exp. time per cycle	6.25 s	1 s
Acquisition time per cycle	3 s	16 ms
Number of cycles	128	96
Experiment time	800 s	96 s
Acquisition time	384 s	1.536 s
Applied field	0.745 MV/cm	0.715 MV/cm
$\frac{SNR_{DCS}}{SNR_{FTIR}}$ with experiment time correction	9.6	
$\frac{SNR_{DCS}}{SNR_{FTIR}}$ with acquisition time correction	52.6	

## Implications and future development/outlook

With the resulting and prospective improvements of the SNR ratio by factors of up to 9.6 or 52.6 using the DCS, it is now interesting to discuss implications for VSS measurements that have not been possible using FTIR spectrometers on a routine basis. One such example is VSS measurements of molecules bound within protein active sites, which provide uniquely different environments relative to glass forming solvents. As a result the Stark response may change if, for instance, the Stark tuning rate is modulated upon substrate or inhibitor binding. Previously, such experiments have only been possible for vibrational probes in the IR-transparent window, e.g. CO bound to the heme of myoglobin<sup>35</sup> or SCN-labelled ketosteroid isomerase<sup>36</sup>, but for other systems poor SNR prevented such studies. The primary barrier towards achieving satisfactory SNRs in such studies is the limited concentration of proteins within a frozen glass matrix of typically up to ca. 1 mM. Therefore, extrapolating from the results of this work, we can see that lowering the solute concentration by 2 orders of magnitude would require an experiment time of 167 h to achieve a Stark spectrum with similar SNR quality as measured during 1 min at 100 mM using FTIR instruments (see Table 2). However, the current DCS setup would be able to reduce this time considerably to roughly 2 h and potentially under constant acquisition of data to <2 min, enabling such experiments to be routine in the future. Note that these numbers were estimated neglecting any spectral overlap with protein signals in the same spectral region.

Table 2. Comparison of performances of two setups used in this study with the prediction of the future DCS instrument under continuous data acquisition. All predictions assume, unless stated otherwise, 100 mM solution of fluorobenzene. All SNR values are referring to an applied field of 1 MV/cm (note signal scales with field squared) and were estimated using a square root dependence of the SNR on time and a linear dependence on concentration.

Feature	FTIR	Dual-comb spectrometer with current acquisition scheme	Potential dual-comb spectrometer with continuous data acquisition
SNR per 1 min experimental time	7.4	71.1	562.4
Experimental time to obtain SNR = 7.4	1 min	0.65 s	10 ms
Experimental time to get SNR = 7.4 at 1 mM	167 h	108 min	104 s
Noise averaged over the spectrum	✓ <sup>1</sup>	✗	✗

<sup>1</sup> only valid when no filters are introduced in the beam path, e.g. to reduce illumination of the detector

Possibility of weighted noise analysis	✗	✓	✓
--	---	---	---

A second common barrier in VSS is presented by restrictions to duration and amplitude of fields that can be applied to a sample before dielectric breakdown. The Stark spectrum, and therefore also the SNR level (see Eq. 1), scales with the applied field squared, so that higher fields could, in principle, drastically shorten experimental times in addition to the previously discussed points. However, practically only routine fields of 1 MV/cm, as used in Table 2, can be applied before high risk of dielectric breakdown becomes a limiting factor with the current FTIR setup and sample configuration. Therefore, one can in principle leverage the high brightness of QCL-based spectrometers to improve the SNR through alterations to the sample, sample-holder, and optical layout. As the FTIR measurements are often photon-limited, an optimal coating of 4.5 nm of Ni and short pathlengths of 25  $\mu\text{m}$  are generally necessary at 100mM sample concentrations. With increased brightness, further tradeoffs in the electrode coating thickness, sample thickness (noting that the signal scales with the applied field squared and only linearly with pathlength), and lowered solute concentration can be considered. In addition, further experimental setups may also be explored through exploiting the higher brightness of the dual-comb spectrometer, such as adjusting the optical layout to transmit the light multiple times through the sample (e.g. by replacing one of the two Ni-coated windows with a mirror and extracting light from the window that was used for illumination). Taken together, the higher brightness and short acquisition and experiment time accessible using the DCS show tremendous promise for increasing the application and feasibility of VSS.

## Conclusions

In this work, we have shown that we can reproduce the Stark spectrum of fluorobenzene using DCS and obtain a Stark tuning rate of  $(0.75 \pm 0.09) \text{ cm}^{-1}/(\text{MV}/\text{cm})$ , which is in line with the result from FTIR measured in this and previous work.<sup>34</sup> Using the DCS, we improved the SNR value of the Stark signal by a factor of 9.6 or 52.6 when taking into account the wavelength-dependent noise for either experimental or acquisition times, respectively. Furthermore, based on the potential of continuous acquisition, which would further improve the SNR, we present future applications that may be accessible using DCS. In conclusion, the DCS provides an experimental setup capable of extending the applications of VSS through fast acquisition, short experiment time, and high brightness. Its spectral sampling of  $0.3 \text{ cm}^{-1}$  brings additional advantage over the conventionally used spectral resolution.

## Acknowledgements

We would like to thank Chi-Yun Lin for helpful discussions. We thank Prof. Ronald Hanson and Dr. Christopher Strand, as well as Prof. Jonathan Fan and Prof. Steven Boxer of Stanford University for providing instrumentation for experiment execution.

## Funding

J. K. acknowledges the Deutsche Forschungsgemeinschaft for a Research Fellowship (KO 5464-1/1). S.H.S. and facilities in the Boxer lab are supported by NIH GM118044.

## Conflict of interest

Authors declare no conflict of interest.

## References

1. S. Fletcher. "The Definition of Electrochromism". *J. Solid State Electrochem.* 2015. 19(11): 3305–3308. 10.1007/s10008-015-3039-9.
2. F.W. Vance, R.D. Williams, J.T. Hupp. "Electroabsorption spectroscopy of molecular inorganic compounds". *Int. Rev. Phys. Chem.* 1998. 17(3): 307–329. 10.1080/014423598230072.
3. B.S. Brunschwig, C. Creutz, N. Sutin. "Electroabsorption spectroscopy of charge transfer states of transition metal complexes". *Coord. Chem. Rev.* 1998. 177(1): 61–79. 10.1016/S0010-8545(98)00188-X.
4. D.R. Borst, T.M. Korter, D.W. Pratt. "On the additivity of bond dipole moments. Stark effect studies of the rotationally resolved electronic spectra of aniline, benzonitrile, and aminobenzonitrile". *Chem. Phys. Lett.* 2001. 350(5): 485–490. 10.1016/S0009-2614(01)01344-6.
5. J. Wilke, M. Wilke, W.L. Meerts, M. Schmitt. "Determination of ground and excited state dipole moments via electronic Stark spectroscopy: 5-methoxyindole". *J. Chem. Phys.* 2016. 144(4): 044201. 10.1063/1.4940689.
6. A. Loukianov, A. Niedringhaus, B. Berg, J. Pan, S.S. Senlik, J.P. Ogilvie. "Two-Dimensional Electronic Stark Spectroscopy". *J. Phys. Chem. Lett.* 2017. 8(3): 679–683. 10.1021/acs.jpcllett.6b02695.
7. A. Chattopadhyay, S.G. Boxer. "Vibrational Stark Effect Spectroscopy". *J. Am. Chem. Soc.* 1995. 117(4): 1449–1450. 10.1021/ja00109a038.
8. S.D. Fried, S.G. Boxer. "Measuring Electric Fields and Noncovalent Interactions Using the Vibrational Stark Effect". *Acc. Chem. Res.* 2015. 48(4): 998–1006. 10.1021/ar500464j.
9. S.D. Fried, S. Bagchi, S.G. Boxer. "Extreme electric fields power catalysis in the active site of ketosteroid isomerase". *Science*. 2014. 346(6216): 1510–1514. 10.1126/science.1259802.
10. S.H. Schneider, S.G. Boxer. "Vibrational Stark Effects of Carbonyl Probes Applied to Reinterpret IR and Raman Data for Enzyme Inhibitors in Terms of Electric Fields at the Active Site". *J. Phys. Chem. B*. 2016. 120(36): 9672–9684. 10.1021/acs.jpcb.6b08133.
11. H. Biava, T. Schreiber, S. Katz, J.-S. Völler, M. Stolarski, C. Schulz, et al. "Long-Range Modulations of Electric Fields in Proteins". *J. Phys. Chem. B*. 2018. 122(35): 8330–8342. 10.1021/acs.jpcb.8b03870.
12. W. Hu, L.J. Webb. "Direct Measurement of the Membrane Dipole Field in Bicelles Using Vibrational Stark Effect Spectroscopy". *J. Phys. Chem. Lett.* 2011. 2(15): 1925–1930. 10.1021/jz200729a.
13. Y. Wu, S.G. Boxer. "A Critical Test of the Electrostatic Contribution to Catalysis with Noncanonical Amino Acids in Ketosteroid Isomerase". *J. Am. Chem. Soc.* 2016. 138(36): 11890–11895. 10.1021/jacs.6b06843.

14. S.D. Fried, S.G. Boxer. "Electric Fields and Enzyme Catalysis". *Annu. Rev. Biochem.* 2017. 86(1): 387–415. 10.1146/annurev-biochem-061516-044432.
15. G. Schkolnik, J. Salewski, D. Millo, I. Zebger, S. Franzen, P. Hildebrandt, et al. "Vibrational Stark Effect of the Electric-Field Reporter 4-Mercaptobenzonitrile as a Tool for Investigating Electrostatics at Electrode/SAM/Solution Interfaces". *Int. J. Mol. Sci.* 2012. 13(6): 7466–7482. 10.3390/ijms13067466.
16. J.G. Patrow, S.A. Sorenson, J.M. Dawlaty. "Direct Spectroscopic Measurement of Interfacial Electric Fields near an Electrode under Polarizing or Current-Carrying Conditions". *J. Phys. Chem. C.* 2017. 121(21): 11585–11592. 10.1021/acs.jpcc.7b03134.
17. J.K. Staffa, L. Lorenz, M. Stolarski, D.H. Murgida, I. Zebger, T. Utesch, et al. "Determination of the Local Electric Field at Au/SAM Interfaces Using the Vibrational Stark Effect". *J. Phys. Chem. C.* 2017. 121(40): 22274–22285. 10.1021/acs.jpcc.7b08434.
18. S.H. Schneider, H.T. Kratochvil, M.T. Zanni, S.G. Boxer. "Solvent-Independent Anharmonicity for Carbonyl Oscillators". *J. Phys. Chem. B.* 2017. 121(10): 2331–2338. 10.1021/acs.jpcc.7b00537.
19. G.U. Bublitz, S.G. Boxer. "STARK SPECTROSCOPY: Applications in Chemistry, Biology, and Materials Science". *Annu. Rev. Phys. Chem.* 1997. 48(1): 213–242. 10.1146/annurev.physchem.48.1.213.
20. D.K. Lambert. "CO on Ni[100]: Stark effect and electroreflectance vibrational spectroscopy". *J. Vac. Sci. Technol. B Microelectron. Process. Phenom.* 1985. 3(5): 1479–1483. 10.1116/1.582971.
21. N.S. Hush, J.R. Reimers. "Vibrational Stark Spectroscopy. 1. Basic Theory and Application to the CO Stretch". *J. Phys. Chem.* 1995. 99(43): 15798–15805. 10.1021/j100043a018.
22. V. Oklejas, C. Sjoström, J.M. Harris. "SERS Detection of the Vibrational Stark Effect from Nitrile-Terminated SAMs to Probe Electric Fields in the Diffuse Double-Layer". *J. Am. Chem. Soc.* 2002. 124(11): 2408–2409. 10.1021/ja017656s.
23. V. Oklejas, C. Sjoström, J.M. Harris. "Surface-Enhanced Raman Scattering Based Vibrational Stark Effect as a Spatial Probe of Interfacial Electric Fields in the Diffuse Double Layer". *J. Phys. Chem. B.* 2003. 107(31): 7788–7794. 10.1021/jp0344693.
24. P. Mondal, M. Meuwly. "Vibrational Stark spectroscopy for assessing ligand-binding strengths in a protein". *Phys. Chem. Chem. Phys.* 2017. 19(24): 16131–16143. 10.1039/C7CP01892D.
25. A. Schliesser, N. Picqué, T.W. Hänsch. "Mid-infrared frequency combs". *Nat. Photonics.* 2012. 6(7): 440–449. 10.1038/nphoton.2012.142.
26. A. Hugi, G. Villares, S. Blaser, H.C. Liu, J. Faist. "Mid-infrared frequency comb based on a quantum cascade laser". *Nature.* 2012. 492(7428): 229–233. 10.1038/nature11620.
27. G. Villares, A. Hugi, S. Blaser, J. Faist. "Dual-comb spectroscopy based on quantum-cascade-laser frequency combs". *Nat. Commun.* 2014. 5. 10.1038/ncomms6192.
28. Y. Wang, M.G. Soskind, W. Wang, G. Wysocki. "High-resolution multi-heterodyne spectroscopy based on Fabry-Perot quantum cascade lasers". *Appl. Phys. Lett.* 2014. 104(3): 031114. 10.1063/1.4862756.
29. S.S. Andrews, S.G. Boxer. "A liquid nitrogen immersion cryostat for optical measurements". *Rev. Sci. Instrum.* 2000. 71(9): 3567–3569. 10.1063/1.1287343.
30. J.L. Klocke, M. Mangold, P. Allmendinger, A. Hugi, M. Geiser, P. Jouy, et al. "Single-Shot Sub-microsecond Mid-infrared Spectroscopy on Protein Reactions with Quantum

Cascade Laser Frequency Combs". *Anal. Chem.* 2018. 90(17): 10494–10500. 10.1021/acs.analchem.8b02531.

31. N.H. Pinkowski, Y. Ding, C.L. Strand, R.K. Hanson, R. Horvath, M. Geiser. "Dual-comb spectroscopy for high-temperature reaction kinetics". *ArXiv190307578 Phys.* 2019.
32. P. Jouy, J.M. Wolf, Y. Bidaux, P. Allmendinger, M. Mangold, M. Beck, et al. "Dual comb operation of  $\lambda \sim 8.2 \mu\text{m}$  quantum cascade laser frequency comb with 1 W optical power". *Appl. Phys. Lett.* 2017. 111(14): 141102. 10.1063/1.4985102.
33. S.S. Andrews, S.G. Boxer. "Vibrational Stark Effects of Nitriles I. Methods and Experimental Results". *J. Phys. Chem. A.* 2000. 104(51): 11853–11863. 10.1021/jp002242r.
34. I.T. Suydam, S.G. Boxer. "Vibrational Stark Effects Calibrate the Sensitivity of Vibrational Probes for Electric Fields in Proteins". *Biochemistry.* 2003. 42(41): 12050–12055. 10.1021/bi0352926.
35. E.S. Park, S.S. Andrews, R.B. Hu, S.G. Boxer. "Vibrational Stark Spectroscopy in Proteins: A Probe and Calibration for Electrostatic Fields". *J. Phys. Chem. B.* 1999. 103(45): 9813–9817. 10.1021/jp992329g.
36. A.T. Fafarman, P.A. Sigala, J.P. Schwans, T.D. Fenn, D. Herschlag, S.G. Boxer. "Quantitative, directional measurement of electric field heterogeneity in the active site of ketosteroid isomerase". *Proc. Natl. Acad. Sci.* 2012. 109(6): E299–E308. 10.1073/pnas.1111566109.

## Supporting Information

Supporting Information containing the steps leading to obtaining the presented results – as parts of our Python code - is available at...

## Corresponding Author:

Urszula Szczepaniak, IRsweep AG, Laubisruestrasse 44, 8712 Staefa, Switzerland

Email: urszula.szczepaniak@irsweep.com

## Supporting information for:

# Vibrational Stark Spectroscopy on Fluorobenzene with Quantum Cascade Laser Dual Frequency Combs

Urszula Szczepaniak<sup>1</sup>, Samuel H. Schneider<sup>2</sup>, Raphael Horvath<sup>1</sup>, Jacek Kozuch<sup>2</sup>, Markus Geiser<sup>1</sup>

<sup>1</sup> IRsweep AG, Laubisruestrasse 44, 8712 Staefa, Switzerland

<sup>2</sup> Department of Chemistry, Stanford University, Stanford, California 94305-5012

## Supporting Information

We present the steps leading to obtaining the presented results – as parts of our Python code. Most of it is focused on DCS data, analogous procedure was implemented for FTIR data.

Step 1. Getting the function describing the absorbance spectrum (pseudo-Voigt):  $A(\tilde{\nu})$ .

Requirements: numpy, matplotlib.pyplot, PseudoVoigtModel from Imfit.models.

- a. Read the IR absorbance spectrum file and prepare the inputs for the model. You need to have wavenumber axis as variable  $x$  and intensity as variable  $y$ .

- b. Fit the data with pseudoVoigt model.

```
mod = PseudoVoigtModel(nan_policy='drop')
pars = mod.guess(y, x=x)
out = mod.fit(y, pars, center=1215, x=x) #1215 is an estimated
wavenumber of the center of the absorbance peak
print(out.fit_report(min_correl=0.25))
out.plot()
```

- c. Save the outputs – you will need them later. Now you can construct a continuous function, that would fit your data. You can check it by:

```
def pVoigt(x, A, mu, sig, alfa):
    return (1-alfa)*A/(np.sqrt(2*np.pi)*sig/np.sqrt(2*np.log(2)))*np.exp(-(x-mu)**2/(2*(sig/np.sqrt(2*np.log(2)))**2))+alfa*A/np.pi*(sig/((x-mu)**2+sig**2))
```



```

x_values = np.linspace(min(x), max(x), 20000)
func = pVoigt(x_values, 0.95622, 1214.2656, 7.306/2, 0.02216) #here are
the values from the fit
plt.plot(x_values, func, 'k')

```

Step 2. Finding derivatives:  $\frac{d}{d\tilde{\nu}} \frac{A(\tilde{\nu})}{\tilde{\nu}}$  and  $\frac{d^2}{d^2\tilde{\nu}} \frac{A(\tilde{\nu})}{\tilde{\nu}}$ . One can also do that manually, but python enables to find analytical formula of the derivatives in a few simple steps, as described below.

Requirements: Symbol, Derivative from sympy.

- a. Declare symbols that you use:
 

```

x = Symbol('x')
Scaling = Symbol('Scaling') # Will be needed later, e.g. to normalize for the
field or extinction coefficient.
alfa = Symbol('alfa')
A = Symbol('A')
sig = Symbol('sig')
mu = Symbol('mu')

```
- b. Define your function [here the above-mentioned pseudo Voigt model] using the declared symbols and find its derivatives:
 

```

function= Scaling*(((1-alfa)*A/(sqrt(2*pi)*sig/sqrt(2*log(2))))*exp(-(x-
mu)**2/(2*(sig/sqrt(2*log(2)))**2))+alfa*A/pi*(sig/((x-mu)**2+sig**2))))/x
#function=sin(x)+5*x+x**2 #if you wish – use something simple to check
whether it works properly

deriv1= Derivative(function, x) # first derivative
deriv2= Derivative(function, x,2) # second derivative
der1 = deriv1.doit()
der2 = deriv2.doit()

```
- c. Display the derivatives to have their analytical formulas.
 

```

print('first der = ')
print(der1)
print('second der = ')
print(der2)

```

Step 3. Fitting the data with the sum of derivatives

Requirements matplotlib.pyplot (below as plt), numpy (as np), scipy.io (as sio), and scipy.optimize (as optimization).

- a. Define the fit formula – use the analytical form you found in step 2. At first, declare A, mu, sig, and alfa, as the values you found by fitting the absorbance spectrum (step 1).

```

def pVoigt(x, A=A, mu=mu, sig=sig, alfa=alfa):
    return Scaling*((1-alfa)*A/(np.sqrt(2*np.pi)*sig/np.sqrt(2*np.log(2)))*np.exp(-(x-
mu)**2/(2*(sig/np.sqrt(2*np.log(2)))**2))+alfa*A/np.pi*(sig/((x-mu)**2+sig**2))))

```

```

def firstDer(x, A, mu, sig, alfa):

```

```

    return x*Scaling*(A*alfa*sig*(2*mu - 2*x)/(np.pi*(sig**2 + (-mu + x)**2)**2) - A*(-
    alfa + 1)*(-2*mu + 2*x)*np.exp(-(-mu +
    x)**2*np.log(2)/sig**2)*np.log(2)**(3/2)/(np.sqrt(np.pi)*sig**3))/x -
    Scaling*(A*alfa*sig/(np.pi*(sig**2 + (-mu + x)**2)) + A*(-alfa + 1)*np.exp(-(-mu +
    x)**2*np.log(2)/sig**2)*np.sqrt(np.log(2))/(np.sqrt(np.pi)*sig))/x**2

```

```

def secondDer(x, A, mu, sig, alfa):
    return x**2*A*Scaling*(4*alfa*sig*(mu - x)**2/(np.pi*(sig**2 + (mu - x)**2)**3) -
    alfa*sig/(np.pi*(sig**2 + (mu - x)**2)**2) - 2*(mu - x)*(alfa*sig/(np.pi*(sig**2 + (mu -
    x)**2)**2) - (alfa - 1)*np.exp(-(-mu -
    x)**2*np.log(2)/sig**2)*np.log(2)**(3/2)/(np.sqrt(np.pi)*sig**3))/x +
    (alfa*sig/(np.pi*(sig**2 + (mu - x)**2)) - (alfa - 1)*np.exp(-(-mu -
    x)**2*np.log(2)/sig**2)*np.sqrt(np.log(2))/(np.sqrt(np.pi)*sig))/x**2 + (alfa -
    1)*np.exp(-(-mu - x)**2*np.log(2)/sig**2)*np.log(2)**(3/2)/(np.sqrt(np.pi)*sig**3) -
    2*(alfa - 1)*(mu - x)**2*np.exp(-(-mu -
    x)**2*np.log(2)/sig**2)*np.log(2)**(5/2)/(np.sqrt(np.pi)*sig**5))/x

```

```

def fit(x, c1, c2, c3):
    return c1*pVoigt(x, A, mu, sig, alfa)+c2*firstDer(x, A, mu, sig,
    alfa)+c3*secondDer(x, A, mu, sig, alfa)

```

- b. Take into account the experimental conditions (here for DCS, analogously for FTIR)

```

path = 28          # optical pathlength in um
ECS = 10000/(0.1*path) # Extinction coefficient scaling [M-1 cm-1]:
10000/(Conc[M]*l[um])
Scaling = ECS      # for the fitting
Field = (2.0/path)*10 # Calculation of the field [MV/cm]: 10*Voltage [kV]/path
[um]
FS = 1/(Field**2)  # Field scaling: 1/Field[MV/cm]^2

```

- c. Load the files, convert to absorbance (taking into account field-on – field-off difference), calculate the difference (half of each acquisition set was with the field on, and half with field off), and crop the FTIR data to have matching regions. Scale the intensity (y axis) with ECS and FS.
- d. Load/find the error values on y axis.
- For DCS data – it is stored in the file, as standard deviation of each laser line intensity under variable *stdPeak* – while using provided postprocessing scripts, can be accessed to with `proc.data['stdPeak']`.
  - For FTIR data, you need to find the error on your own – cut out a part of the spectrum without spectral features, and fit it with the straight line. Use RMSE as an error.
- e. Fit the data to the sum of derivatives. Inputs: fit – as defined before, Xax – x-axis, Int – intensity (y-axis), x0 – initial guess of parameters (here: `x0 = np.array([0, 0, 0])`).

```

errors = np.copy(STD) # Read standard deviation as errors for the DCS weighted fit
params, params_covariance = optimization.curve_fit(fit, Xax, Int, x0, sigma=errors,
absolute_sigma=True) # absolute_sigma refers to the fact that exact values of
standard deviation are used, without additional normalization; for FTIR, sigma and
absolute_sigma are not specified and used as default. See below.

```

```

"""sigma : None or M-length sequence or MxM array, optional
    Determines the uncertainty in ydata. If we define residuals as  $r = ydata - f(xdata, *popt)$ , then the interpretation of sigma depends on its number of dimensions:
    A 1-d sigma should contain values of standard deviations of errors in ydata. In this case, the optimized function is  $chisq = \sum((r / sigma) ** 2)$ .
    A 2-d sigma should contain the covariance matrix of errors in ydata. In this case, the optimized function is  $chisq = r.T @ inv(sigma) @ r$ .
    New in version 0.19.
    None (default) is equivalent of 1-d sigma filled with ones.
"""

```

```

yfitDCS = fit(Xax, params[0], params[1], params[2])

```

Step 4. Finding the Stark tuning rate

```

a. Calculate the Stark tuning rate
DmuDCS = np.sqrt(10*params[2])
b. Calculate the uncertainty on the Stark tuning rate
paramsErr = np.sqrt(10*np.sqrt(np.diag(params_covariance)))
c. The Stark tuning rate is DmuDCS +/- paramsErr[2]

```

Step 5. Finding the SNR

```

weight = 1/(STD**2) # inverse variance, for FTIR it was an array of 1: weight = yf/yf
Error = np.sum(weight*STD)/np.sum(weight) # in FTIR: Error_FT =
np.sum(weight*rmse)/np.sum(weight)
sigD = max(yfitDCS)-min(yfitDCS) # signal DCS – from the fit not to rely on noisy
data points.
SNR = sigD/Error # SNR defined as maximal signal divided by the error over the
whole probed part of the spectrum

```